Noise Characterization of Femtosecond Fiber Raman Soliton Lasers

URSULA KELLER, KATHRYN D. LI, MARK RODWELL, AND DAVID M. BLOOM, FELLOW, IEEE

Abstract—**We have measured the broad-band amplitude noise and the phase noise (timing jitter) of femtosecond fiber Raman soliton lasers. For a single-pass compressor using 300 m of either standard single-mode fiber or polarizing preserving fiber, we measure white (flat with frequency) amplitude noise ≥50 dB above shot noise at 2 mA photocurrent, for frequencies higher than approximately 100 kHz. This is ≈30 dB larger than the amplitude noise observed from fiber grating pulse compressors. The timing jitter increases with pump power, and at 1.6 W pump power, we have measured 5.2 ps rms timing jitter, given ≈2 ps jitter from the Nd:YAG pump. Longer fibers in the single-pass compressor do not affect the amplitude noise, but increase the timing jitter even further. A synchronously pumped ring cavity reduced the timing jitter substantially, but did not significantly improve the amplitude noise. The high amplitude noise of these systems makes their use unattractive for detection of signals with a small modulation depth, such as in electrooptic sampling. However, the simple single-pass compressor may find application in optical pump–probe experiments which have larger signal levels.**

I. Introduction

FIBER Raman soliton lasers have been extensively used to generate near-infrared femtosecond pulses at wavelengths around 1.3 μm. In these lasers, picosecond laser pulses are launched into a single-mode optical fiber, generating Raman-shifted pulses [1] that are compressed by the soliton effect [2]. Gouveia-Neto *et al.* [3], using a CW mode-locked Nd:YAG laser at 1.32 μm as a pump source, reported tunable 1.3–1.5 μm femotosecond (<100 fs) pulses. In a similar experiment, Kafka *et al.* [4] generated 160 fs pulses. Islam *et al.* [5] obtained 250 fs pulses with a two-fiber ring cavity configuration pumped by 10 ps pulses from a color center laser. Zysset *et al.* [6] obtained a minimal pulse width of 77 fs tunable over 1.37–1.49 μm using 1 ps long pulses from a synchronously pumped infrared dye laser. The focus of these papers is on the minimum pulse width and the pulse shape measured with optical autocorrelators; however, little attention has been paid to the laser's amplitude and timing stability. These parameters are important in the application of lasers to physical experiments.

Our interest in these lasers is their potential application in optical sampling systems to measure the applied voltage [7] in GaAs devices and sheet charge densities in Si [8] and GaAs [9] devices with a subpicosecond time resolution. For these and similar experiments, in addition to a short and stable pulse autocorrelation, the laser pulses must have negligible pedestals, small low-frequency amplitude noise, very low background amplitude noise at higher frequencies, and in some experiments, stable pulse timing. The shape of the observed pulses from a fiber Raman soliton laser consists typically of a short pulse superimposed upon a much longer lower-amplitude pulse commonly referred to as a "pedestal." The pedestal results in an undesired variation in the frequency response in sampling measurements, at frequencies on the order of the inverse of the pedestal time duration. In optical probing experiments, where a laser probe beam intensity is modulated in proportion to a variable under measurement, low-frequency amplitude fluctuations occurring within the signal detection bandwidth result in fluctuations in the measurement; therefore, small low-frequency amplitude noise is required. Laser amplitude noise typically falls off with increased frequency. Therefore, the experimental signal-to-noise ratio is increased by translating the detected signal to higher frequency using chopping techniques. The background amplitude noise at the chopping frequency determines the minimum detectable signal for a given acquisition time. While timing jitter (or phase noise) is not important in optical pump–probe experiments, low timing jitter is essential for experiments involving synchronization of the laser pulse repetition rate with a microwave generator or experiments synchronizing two lasers. Jitter in sampling experiments degrades the time resolution and gives rise to additional noise in the measurement.

We have constructed a single-pass fiber Raman soliton compressor and a synchronously pumped fiber Raman soliton ring laser, pumped with a second harmonic mode-locked Nd:YAG laser at 1.32 μm [10], similar to that in Taylor's and Kafka's approach and have reproduced their results in terms of pulse width (≤ 200 fs). In this paper, we concentrate on the characterization of the amplitude noise and phase noise (timing jitter) of these lasers. The actual physical effects that are responsible for the laser fluctuations are not discussed in great detail. Such a discussion is beyond the scope of this paper.

II. Noise Measurements

We use power spectrum techniques to measure laser amplitude and phase noise, well-known techniques in the

Manuscript received July 29, 1988; revised October 11, 1988. This work was supported in part by the U.S. Office of Naval Research under Contract N00014-86-0530, in part by an IBM Predoctoral Graduate Fellowship, and in part by a John Hertz Foundation Fellowship.

The authors are with the Edward L. Ginzton Laboratory, Stanford University, Stanford, CA 94305.

IEEE Log Number 8825915.

characterization of microwave synthesizers and other microwave instruments [11]–[13]. The same techniques also have been used to characterize the noise of CW mode-locked lasers [14], [15] and synchronously mode-locked dye lasers [16]; however, they are still not widely used in the optics community, where mostly only autocorrelations and cross correlations are used to characterize laser performance. We will give an overview of power spectrum techniques after discussing the limitations of autocorrelation and cross-correlation methods in inferring the amplitude and phase stability.

Conclusions from a "structureless" autocorrelation usually give inadequate information about amplitude noise because the bandwidth of the receiver (the photomultiplier and its circuit) is limited. No information on the higher-frequency background intensity noise and the timing jitter of the laser can be gained. Optical cross correlations are sometimes used to investigate the timing jitter of pulsed lasers. For a laser with a pulse repetition period of 10 ns, a cross correlation of two consecutive pulses will not measure timing jitter frequency components below about 25 MHz. As we will show, the timing jitter spectrum typically rolls off at a frequency lower than 100 kHz. For typical laser experiments, laser pulse timing variations occurring over a period of 1–10 s are of concern, requiring a cross-correlation delay of about 1–10 s, which corresponds to about a 10^8–10^9 m optical delay line in the cross correlator.

The laser intensity $I(t)$ is a pulse train with an average power P, a pulse repetition period T, a normalized laser power fluctuation $N(t)$, and a timing jitter described by the random variable $J(t)$ for the pulse arrival time. For analysis of the laser power spectrum given amplitude and phase (timing) noise, we can treat the pulses as delta functions:

$$I(t) = PT\big[1 + N(t)\big] \sum_{-\infty}^{\infty} \delta\big(t - nT - J(t)\big). \quad (1)$$

A photodetector and a spectrum analyzer are used for noise measurements. Spectrum analyzers display the power spectral density $S_p(\omega)$ integrated over the analyzer resolution bandwidth. $S_p(\omega)$ is the Fourier transform of the statistical autocorrelation function of $I(t)$. With the assumption that the amplitude noise and the timing jitter are ergodic (the time average is the same as the ensemble average) and stationary, the power spectral density is given by

$$S_p(\omega) = F\big\{I(t) \star I(t)\big\} \quad (2)$$

where F stands for the Fourier transformation and $\star$ is the correlation operator. It follows then that

$$S_p(\omega) = P^2 \sum_{n=-\infty}^{\infty} \big[2\pi\delta(\omega - n\omega_L) + S_N(\omega - n\omega_L) + n^2\omega_L^2 S_J(\omega - n\omega_L)\big] \quad (3)$$

where we used the identity

$$\sum_{n=-\infty}^{\infty} \delta\big(t - nT - J(t)\big) = \frac{1}{T}\sum_{n=-\infty}^{\infty} \exp\big(jn\omega_L\big(t - J(t)\big)\big) \quad (4)$$

and expanded to first order in $J(t)$. $S_N(\omega)$ is the amplitude noise spectral density, and $S_J(\omega)$ is the phase noise spectral density repeated at each harmonic of the pulse repetition rate $\omega_L = (2\pi)/T$. By expanding (4) to second order in $J(t)$, it can be shown that the timing jitter also degrades the bandwidth of the sampling measurement using these pulses [15]. Additionally, pulse shape fluctuations appear as higher-order terms in $n\omega_L$ and are neglected in (3). The rms amplitude fluctuation σ_N [standard deviation of $N(t)$] is given by

$$\sigma_N^2 = \big\langle N^2(t)\big\rangle = \frac{1}{\pi}\int_0^{\infty} S_N(\omega)\, d\omega, \quad (5)$$

and similarly for the rms timing jitter σ_J using $S_J(\omega)$ where $\langle \cdots \rangle$ is the mean value.

For the rms value given in (5), no assumptions of the specific statistics of the random variables $N(t)$ and $J(t)$ are made. From (3), it follows that the normalized amplitude-noise sidebands are constant in magnitude with increasing harmonics of the laser repetition rate. Typically, the amplitude-noise sidebands dominate at lower laser harmonics, while the phase-noise sidebands, having power proportional to n^2, dominate for harmonics of higher order. Thus, amplitude noise is determined by measuring the sidebands on a low laser harmonic, while timing jitter (phase noise) is determined by measurements on a sufficiently high harmonic. For the timing jitter measurement, it has to be verified that the chosen high-harmonic-noise sidebands are not dominated by amplitude noise. Fig. 1 shows measured noise sidebands of the fiber Raman soliton compressor at the 23rd and 50th laser harmonic. The measured 6.8 dB increase is predicted by (3) and demonstrates that the noise sidebands at the 50th laser harmonic are dominated by phase noise.

In measurement, σ_N and σ_J are determined in a finite bandwidth $[\omega_{\text{low}}, \omega_{\text{high}}]$, and the integration in (5) runs only over this frequency range:

$$\sigma_N = \sqrt{\big\langle N(t)^2\big\rangle} = \sqrt{\frac{1}{\pi}\int_{\omega_{\text{low}}}^{\omega_{\text{high}}} S_N(\omega)\, d\omega}, \quad (6)$$

and similarly for σ_J. The measurement duration ΔT determines ω_{low} because the mean-squared change in the normalized laser intensity over a time duration of ΔT is given by

$$\big\langle \big(N(t + \Delta T) - N(t)\big)^2\big\rangle = \frac{2}{\pi}\int_0^{\infty} S_N(\omega)\big(1 - \cos(\omega\Delta T)\big)\, d\omega. \quad (7)$$

The same equation is valid for the timing jitter, using $J(t)$

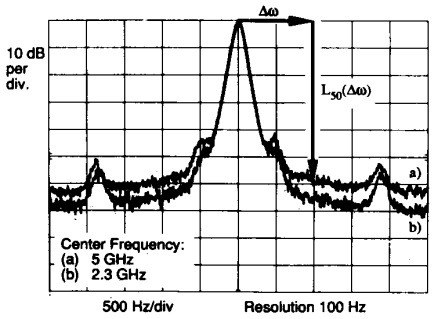

Fig. 1. Spectrum analyzer display of noise sidebands at the 23rd and the 50th laser harmonic from the single-pass compressor.

instead of $N(t)$ and S_J instead of S_N. Because $(1 - \cos(\omega\Delta T))$ varies as $(\omega\Delta T)^2$ for $(\omega\Delta T) << 1$, amplitude fluctuations and timing jitter components with frequencies below $\omega_{\text{low}} = \pi/2\Delta T$ contribute little to changes in the laser intensity and timing observed over the period ΔT. For this reason, the cross correlation of two pulses 10 ns apart gives no information of the timing jitter below about 25 MHz. The detection bandwidth of the measurement determines ω_{high}. Very often, the phase-noise sidebands cannot be measured over the entire frequency span because they roll off below the amplitude-noise sidebands even at high laser harmonics.

The spectrum analyzer displays power density $P(f)$, integrated over the resolution bandwidth B, as a function of the frequency f. The peak of the spectrum is at a harmonic of the oscillation frequency, referred to as the carrier power P_c (see as an example Figs. 1 and 4). From (3) and the spectrum analyzer display, the amplitude fluctuation for a given frequency span $[f_{\text{low}}, f_{\text{high}}]$ is given by

$$\sigma_N[f_{\text{low}}, f_{\text{high}}] = \sqrt{\frac{P_{sb}}{P_c}}$$

with

$$P_{sb} = 2\int_{nf_L + f_{\text{low}}}^{nf_L + f_{\text{high}}} \frac{P(f)}{B}\, df, \tag{8}$$

and the timing jitter is given by

$$\sigma_J[f_{\text{low}}, f_{\text{high}}] = \frac{T}{2\pi n}\sqrt{\frac{P_{\text{sb}}}{P_c}} \tag{9}$$

where B is the resolution bandwidth of the spectrum analyzer, n is the harmonic number of the measured sidebands, and f_L is the laser repetition frequency.

Except in squeezed-state [17] experiments, the laser intensity noise is larger than the shot noise power. The excess noise $S_N(\omega)$ can be stated as the excess of the shot noise power given in decibels above the shot noise at a given photocurrent. At the photodetector, the ratio of shot noise power P_{SN} to the carrier power P_c is

$$\frac{P_{\text{SN}}}{P_c} = \frac{2qB}{I_0} \tag{10}$$

where B is the resolution bandwidth of the measurement, I_0 is the dc photocurrent, and q is the electronic charge. Alternatively, the excess laser noise $S_N(\omega)$ in a 1 Hz bandwidth can be stated with respect to the carrier power. In this case, the units of $S_N(\omega)$ are given in dBc (1 Hz), i.e., the decibels below the carrier in a 1 Hz bandwidth. The detector dc photocurrent I_0 is proportional to the average laser power. The shot noise power is proportional to I_0, whereas the carrier and the excess noise power are both proportional to I_0^2 [see (3)]. For this reason, the excess laser noise in units of dBc (1 Hz) is independent of the photocurrent, provided that the noise sidebands are not shot noise limited. The phase noise is also stated as the sideband power relative to the carrier by the single-sideband phase-noise spectral density of the laser nth harmonic, $L_n(\omega) = n^2\omega_L^2 S_J(\omega)$. This parameter, used to specify the stability of microwave oscillators, is defined in Fig. 1. The units of $L_n(\omega)$ are given in dBc (1 Hz). Measurements of $L_n(\omega)$ and $S_N(\omega)$ as described are independent of the receiver system characteristics, provided that the noise sidebands are both above the measurement system noise level and measured over a frequency range where the receiver's response is flat.

III. Single-Pass Fiber Raman Soliton Compressor

The simplest fiber Raman soliton laser is the single-pass compressor, where pump pulses are Raman shifted and compressed by the soliton effect while propagating through the fiber. At the fiber output, a polarizer and a dichroic mirror separate the 1.32 μm pump from the Raman-shifted short pulse. The dichroic mirror is a dielectric high-pass filter with a cutoff wavelength determined by the angle of incidence. We use 300 m of standard single-mode fiber and 300 and 700 m of polarization-preserving single-mode fiber with a dispersion minimum around 1.3 μm. The calculated walkoff distance between the 55 ps 1.32 μm pump pulse and the short 1.4 μm Raman-shifted pulse is 160 m. The 300 m fiber length is chosen because the maximum Raman signal is achieved with a fiber length of 1.5 to 2 times the walkoff distance [18]. A 30 dB optical Faraday isolator isolates the pump laser from fiber feedback. An AR-coated 10X focusing lens couples into the fiber with $\approx$60 percent efficiency. A fiber polarization controller [11] and the tunable high-pass filter (dichroic mirror) are used to suppress the pedestal.

For full diagnostics of the compressed pulses, we used the following equipment. A quarter-meter 0.5 nm resolution monochromator monitors the pulse spectrum. A noncollinear optical autocorrelator with a scanning 8 cm optical delay, capable of measuring 50 ps Gaussian pulses with 2.7 percent linearity, measures the compressed pulse and its pedestal. A Hewlett-Packard HP8566 spectrum analyzer (with a minimum resolution bandwidth of 10 Hz) and an HP3561A dynamic signal analyzer (with a minimum resolution bandwidth of $\approx$0.6 mHz) with a photodiode measures the laser noise spectrum. An InGaAs photodiode and sampling scope (40 ps FWHM combined impulse response) provide qualitative real-time observa-

tions of the laser noise while varying the experimental parameters.

A second harmonic intensity optical autocorrelator gives the pedestal width and height as a function of the optical delay time, and we use this information to approximate the percentage of the total energy contained in the compressed short part of the uncorrelated pulse. Fig. 2 shows the autocorrelation over a narrow and a wide span of a compressed pulse with a long pedestal. From the 9.6 ps span [Fig. 2(b)], a 260 fs FWHM autocorrelated pulse duration is determined. From the wider 240 ps span, we find that only 5.4 percent of the total energy is contained within the compressed short pulse. We were able to suppress the pedestal significantly with a tunable high-pass filter by decreasing the angle of incidence to the dichroic mirror. Decreasing the angle of incidence from 55 to 20°, the percentage of the total energy contained in the compressed short part of the pulse increased from 5.4 percent to more than 75 percent. Fig. 3(a) shows the autocorrelation of a pulse with the pedestal significantly suppressed using a 30° angle of incidence to the dichroic mirror, giving 46 percent of the total energy in the short pulse. The effect on the spectrum is shown in Fig. 3(b), where the 55° angle of incidence corresponds to the pulse shown in Fig. 2, and the 30° angle of incidence corresponds to the pulse in Fig. 3(a). By filtering successively more of the shorter-wavelength part of the spectrum, the pedestal is reduced, and the percentage of the total pulse energy contained in the short compressed pulse is increased. This implies that the short compressed pulse dominantly consists of the longer-wavelength tail of the pulse spectrum. Similar spectral modification was observed when the fiber polarization controller was used to suppress the pedestal. Using both the fiber polarization controller and the adjustable high-pass filter, we were able to suppress the pedestals sufficiently, fulfilling one requirement for the laser's application in optical sampling experiments.

We measured the amplitude noise on the 300 m fiber at three different input power levels; close to threshold with an input pump power P_{in} of 0.9 W and an average Raman-shifted power P_r of approximately 5 mW after the dichroic mirror, at P_{in} = 1.3 W with P_r = 70 mW corresponding to 24 percent Raman conversion, and at P_{in} = 1.6 W with P_r = 170 mW corresponding to 47 percent Raman conversion. The dichroic mirror angle of incidence was kept constant at 50°. Fig. 4 displays the measured amplitude-noise sidebands at a 10 MHz frequency span measured with a Ge photodetector and the spectrum analyzer with 100 kHz resolution bandwidth at all three input power levels. By blocking the beam, we verified that the measurement was not limited by the measurement system noise [see Fig. 4, trace (a)]. The shot noise power level with 100 kHz resolution bandwidth is at −108 dBc at I_0 = 2 mA [eq. (10)]. At 2 mA photocurrent,the amplitude sidebands are (b) 54 dB above shot noise at P_{in} = 1.6 W, (c) 58 dB above shot noise at P_{in} = 1.3 W, and (d) 68 dB above shot noise at P_{in} = 0.9 W. Below ≈ 100 kHz offset, larger low-frequency amplitude fluctuations

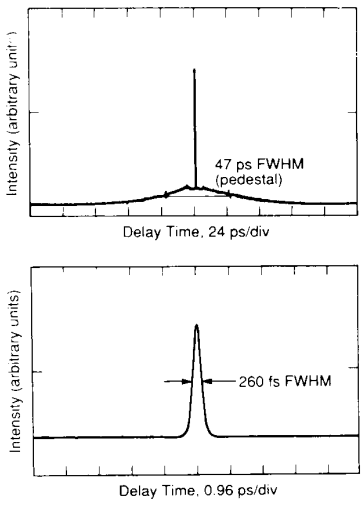

Fig. 2. Measured autocorrelation traces of a compressed pulse with large pedestal.

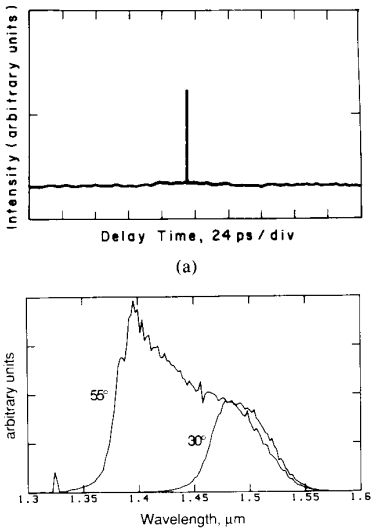

Fig. 3. (a) Autocorrelation of a pulse with substantially suppressed pedestal (30° angle of incidence to the dichroic mirror), where 46 percent of the total pulse energy is contained in the short pulse. (b) Pulse spectrum for 55 and 30° angle of incidence to the dichroic mirror.

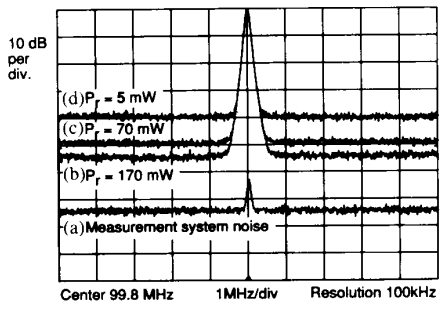

Fig. 4. High-frequency amplitude-noise sidebands of a 300 m fiber Raman soliton compressor at different pump powers. Trace (b)—P_{in} = 1.6 W; trace (c)—P_{in} = 1.3 W; trace (d)—P_{in} = 0.9 W. Trace (a) shows the measurement system noise determined by blocking the beam.

are observed. The amplitude noise of the CW mode-locked Nd:YAG pump laser shows a typical $1/f$ rolloff with increased frequency offset from the carrier, approaching the shot noise level after a few hundred kilohertz frequency offset. The low-frequency amplitude noise below ≈ 100 kHz of the fiber Raman soliton compressor is typically 10–30 dB larger than the pump laser noise, with the same spectral structure.

Fig. 5 displays the amplitude noise between two consecutive laser harmonics separated by the 99.8 MHz laser repetition frequency and demonstrates that the high-frequency amplitude noise is white (flat with frequency). In Fig. 5, the laser was operated under the same conditions, with 1.3 W input pump power, as in Fig. 4(c), but was measured with an ≈ 18 GHz InGaAs photodiode at a dc photocurrent of 0.1 mA. Both traces show -100 dBc (1 Hz) amplitude noise, independent of the detector and photocurrent (see Section II).

By decreasing the angle of incidence of the dichroic mirror to suppress the pedestals, we observed a further increase in the amplitude noise shown in Fig. 6 for two different input powers. Unfortunately, greater pedestal suppression is accompanied by increased amplitude noise. We also used 300 m of polarization-preserving fiber, for which we observed approximately the same noise properties. Increasing the fiber length to 700 nm did not change the amplitude noise significantly. The white noise sidebands in this case were around 55–60 dB above shot noise ($I_0 = 2$ mA) and increased to 72 dB above shot noise ($I_0 = 2$ mA) close to the Raman threshold.

The phase noise shows significant structure at frequencies approaching the 10 Hz resolution of the microwave spectrum analyzer. Therefore, the higher-resolution dynamic signal analyzer is used. Microwave-frequency laser harmonics are translated to a 50 Hz difference frequency using a microwave mixer and a low-phase-noise synthesizer (an HP8340A). We measured the phase-noise sidebands at the 60th harmonic of the 99.8 MHz repetition rate at about 5.9 GHz with the higher-resolution dynamic signal analyzer. At this frequency, the phase noise dominates the noise sidebands, which was experimentally confirmed by the predicted [eq. (3)] 8.3 dB increase of the sidebands between the 23rd (≈ 2.3 GHz) and the 60th laser harmonic (≈ 5.9 GHz). Fig. 7 shows the single-sideband phase-noise spectral density of the Nd:YAG laser, reduced to the 99.8 MHz laser fundamental $L_1(f)$ in dBc (1 Hz), covering a frequency span from 25 Hz to 5 kHz. The timing jitter over the frequency span of (25 Hz, 5 kHz) is 2 ps rms [eq. (9)]. Fig. 8 displays $L_1(f)$ over the same frequency span for the 300 m fiber Raman soliton compressor at 1.6 and 1.4 W pump power, with the dichroic mirror angle of incidence fixed at 50°. The phase noise much below 25 Hz offset is dominated by phase drift between the mode-locker driver and the microwave synthesizer used in the measurement, and the phase noise above 5 kHz offset begins to fall below the relatively high-amplitude-noise sidebands, even when measured on laser harmonics approaching the bandwidth

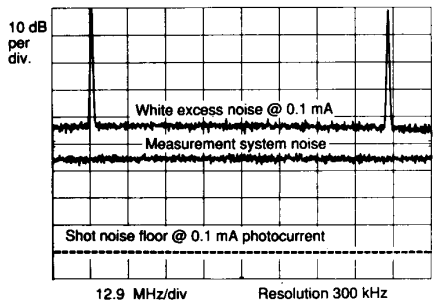

Fig. 5. White amplitude noise of the fiber Raman soliton compressor displayed over two consecutive laser harmonics, measured at 0.1 mA dc photocurrent.

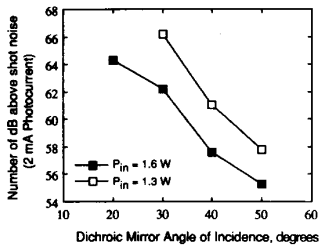

Fig. 6. Amplitude noise in function of the angle of incidence to the dichroic mirror. Better pedestal suppression with decreased angle of incidence results in higher amplitude noise.

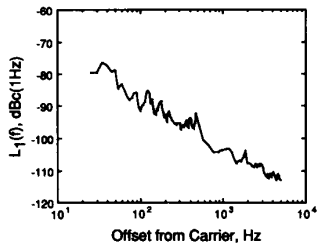

Fig. 7. Single-sideband phase-noise spectral density $L_1(f)$ of the YAG pump laser at the laser fundamental.

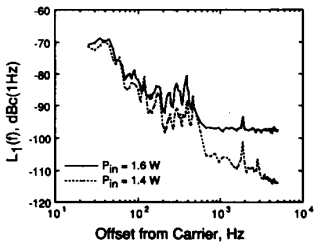

Fig. 8. Single-sideband phase-noise spectral density $L_1(f)$ of the single-pass fiber Raman soliton compressor using 300 m fiber.

of the InGaAs photodiode. At lower pump powers below 1.4 W, it becomes increasingly difficult to measure the phase noise due to the even further increased amplitude noise, which dominates the noise sidebands. The timing jitter in a (25 Hz, 5 kHz) of the fiber Raman soliton com-

pressor is 5.2 ps rms at a pump power P_{in} of 1.6 W and 3.9 ps rms at P_{in} = 1.4 W, given the 2 ps timing jitter from the Nd:YAG pump. Assuming a Gaussian distribution, the 5.2 ps rms timing jitter corresponds to a pulse timing distribution of 12.3 ps FWHM.

The fiber compressor timing jitter is larger with increased pump power and increases drastically for a longer 700 m fiber. The phase noise of the pump laser and of the 300 m fiber compressor with 1.4 W input power quickly rolls off with increasing frequency offset to the carrier (Figs. 7 and 8). At a higher 1.6 W pump power, the 300 m fiber compressor shows noise sidebands leveling off above ≈ 600 Hz (Fig. 8). The high-frequency phase noise is enhanced for the longer 700 m fiber compressor [Fig. 9(a)]. Because the experimental conditions do not satisfy the approximations required for the validity of (3), the observed 20 dB difference in the noise power between the harmonics at 2.3 and 5 GHz is much more than the predicted 6.8 dB increase. In particular, the high laser amplitude noise forces phase measurements at high laser harmonics, at which the small-angle condition assumed for (3) is violated. The observed noise sidebands might also arise from multiple pulsing, which is not modeled by (1) and (3). Under these conditions the measured compressor output observed on a fast photodetector and a sampling scope with a combined 40 ps impulse response shows large instabilities [Fig. 9(b)]. In contrast, the autocorrelation pulse [Fig. 9(b)] is stable. Fig. 9 clearly demonstrates that an autocorrelator alone is insufficient for a full diagnostic of the laser noise properties.

The described single-pass fiber Raman soliton compressor is a very simple approach for achieving sub-300 fs pulses with good pedestal suppression. However, the observed amplitude noise is much higher than observed for a standard fiber grating pulse compressor, where at 1 MHz carrier offset the excess noise was ≈ 20 dB above shot noise (I_0 = 2 mA) [7]. For optical pump–probe experiments, for which timing jitter is of no concern, the determined amplitude fluctuations still allow measurements of larger signals with very good time resolution. For example, by using chopping techniques to leave the region of the higher low-frequency amplitude noise, the white excess noise of 54 dB above shot noise at 2 mA photocurrent [Fig. 4, trace (b)] corresponds only to 0.2 percent rms amplitude fluctuation within a 50 kHz bandwidth. Small signal measurements, such as in optical sampling measurements, require better noise properties. For example, an excess noise level of 51 dB above shot noise (I_0 = 1 mA) increases the minimum detectable voltage in electrooptic sampling sampling from 30 $\mu V/\sqrt{1}$ Hz in the shot noise limit to 10 mV/$\sqrt{1}$ Hz and the minimum detectable sheet charge density in optical charge-sensing measurements in GaAs devices from $2.3 \cdot 10^7$ cm$^{-2}/\sqrt{1}$ Hz in the shot noise limit to $8 \cdot 10^9$ cm$^{-2}/\sqrt{1}$ Hz. We expect that synchronously pumped fiber Raman soliton lasers, where stimulated Raman conversion dominates spontaneous Raman conversion, should exhibit better noise performance.

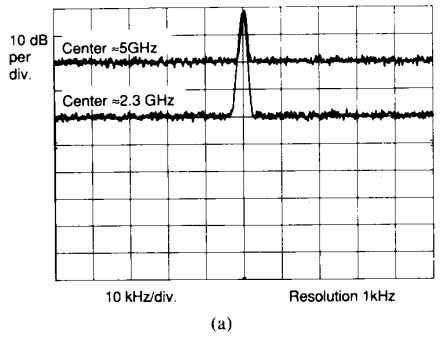

(a)

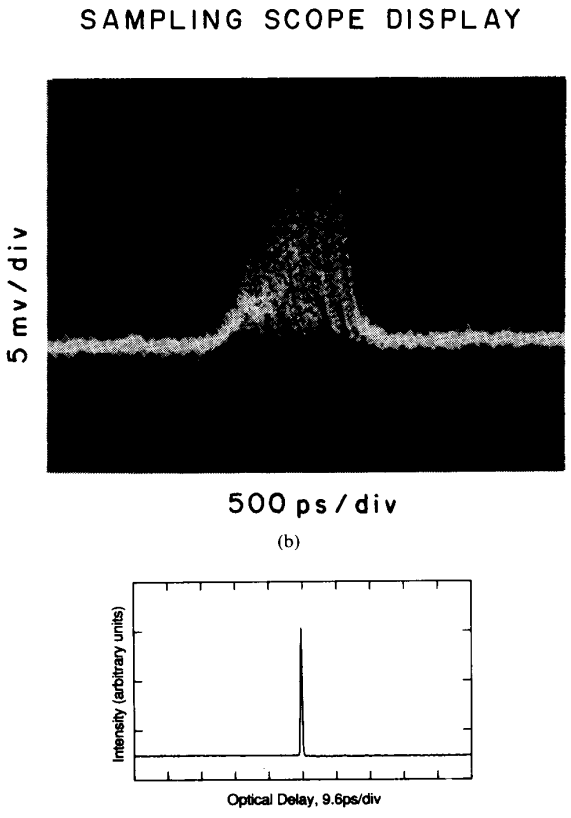

(b)

(c)

Fig. 9. Monitored pulses from a single-pass compressor (700 m of fiber). (a) Microwave spectrum analyzer display (noise sidebands). (b) Sampling scope display (using a fast detector giving 40 ps FWHM combined impulse response). (c) The optical autocorrelation.

IV. Fiber Raman Soliton Ring Laser

A synchronously pumped ring laser is expected to show better amplitude and timing stability than the single-pass compressor discussed in Section III. As a first experiment to demonstrate its better noise performance, we used a relatively low-Q ring cavity. The high loss in the cavity is dominated by the 40 percent fiber coupling loss. A fully integrated fiber-loop cavity would be necessary to decrease the cavity losses substantially.

The synchronously pumped ring cavity is shown in Fig. 10, following closely the original approach of Islam *et al.*

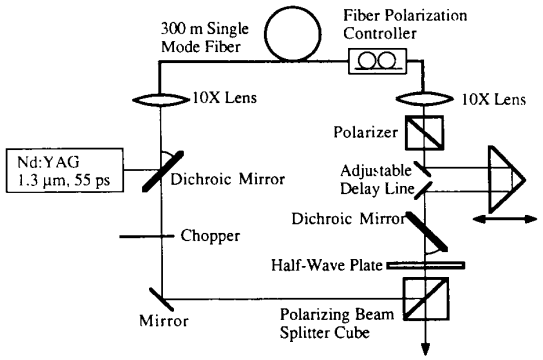

Fig. 10. Experimental setup of a synchronously pumped fiber Raman soliton laser. The chopper is used only during cavity alignment.

[5]. The pump pulse from a second harmonic mode-locked Nd:YAG laser is coupled into the ring cavity with another dichroic mirror at a fixed 55° angle of incidence. At the output of a 300 m standard single-mode fiber, a dichroic mirror serves as a tunable high-pass filter for the s-polarization; the p-polarization is previously rejected by a polarizer. A half-wave plate and the polarizing beam splitter form an adjustable output coupler, giving a p-polarized output beam. During cavity alignment, the feedback into the fiber is mechanically chopped, and the ring laser output intensity is monitored by a photodiode and a lock-in amplifier. The chopper is then removed. Rough synchronization was achieved by monitoring the ring laser output with a fast InGaAs photodiode and the sampling scope (40 ps FWHM combined impulse response) and by trimming the fiber length so that the Raman-shifted pulse and the relaunched pulse overlapped on the sampling scope display. A roof prism and a translation stage as a variable delay line provides fine cavity tuning. Because of the high cavity losses, cavity synchronization was noncritical. For full diagnostics of the compressed pulses, we used the same tools described in the previous section.

We observed reduced amplitude and phase noise with the synchronously pumped ring cavity. Input power and feedback were adjusted to minimize the amplitude noise. The best amplitude noise of 45 dB above shot noise (I_0 = 2 mA) was achieved at input powers very close to the single-pass compressor threshold (250 mW output power with 400 mW pump power). The white excess amplitude-noise power of 45 dB above shot noise is still about 25 dB greater than the standard fiber grating compressor. When we increase the pump power, the amplitude noise increases and finally approaches the noise level of a single-pass compressor. We believe that a higher-Q cavity will further decrease the excess amplitude noise.

As expected, at input powers very close to the single-pass compressor threshold, the measured timing jitter was determined by the pump laser, and we measured 2 ps rms in a (25 Hz, 5 kHz) bandwidth, matching the 2 ps timing jitter of the YAG pump laser.

Operated under the conditions which minimize amplitude noise, substantial pedestal power is observed. The autocorrelation shows a pedestal with a 29 percent amplitude and 60 ps duration; hence, the total pedestal energy is large, containing ≈ 97 percent of the total energy. This is a substantial increase of the pedestal in comparison to the single-pass compression. The monochromator scan (Fig. 11) of the synchronously pumped laser output shows a much narrower spectral line than observed with the single-pass configuration [Fig. 3(b)]. In contrast to the single-pass compressor, a wavelength discrimination between the short compressed pulse and the pedestal was not observed, and we could not apply the previously used methods for pedestal suppression using a high-pass filter or a fiber polarization controller.

V. Conclusions

For a single-pass fiber Raman soliton compressor with 300 m of standard single-mode fiber, we typically obtained sub-300 fs pulses and suppressed the pedestal substantially using a high-pass filter and a fiber polarization controller. The energy contained in the short pulse could be increased to more than 75 percent. The amplitude noise of the CW mode-locked Nd:YAG pump laser shows a typical $1/f$ rolloff with increased frequency offset from the carrier, approaching the shot noise level after a few hundred kilohertz frequency offset. In the single-pass fiber Raman soliton compressor, the low-frequency amplitude noise (< 100 kHz offset from the carrier) is typically 10–30 dB larger than the pump laser noise with the same spectral structure, which implies that these components of amplitude fluctuations are correlated and are determined by the pump laser. At higher frequencies, the noise is flat with frequency ("white"), which implies uncorrelated pulse–pulse amplitude fluctuations. The excess noise is ≥ 50 dB above the 2 mA shot noise power, which is ≥ 30 dB more than the excess noise at 1 MHz offset observed from a fiber grating pulse compressor. The timing jitter increases to 5.2 ps rms with increasing pump power (1.6 W maximum), given 2 ps jitter from the Nd:YAG pump. Using polarization-preserving fiber did not change the noise properties of the laser. A longer fiber (700 m) increases the timing jitter substantially, whereas the amplitude noise remains the same.

First experiments with a synchronously pumped fiber Raman soliton laser were done with a relatively low-Q cavity including a 40 percent fiber coupling loss. The measured high-frequency amplitude noise was decreased to 45 dB above 2 mA shot noise power. The timing jitter was reduced to the level of the fluctuations of the pump laser. The pedestal increased significantly, and we were unable to suppress it with a high-pass filter or a polarization controller.

We believe that the observed uncorrelated excess amplitude noise is due to the spontaneous Raman conversion because the pump laser has no uncorrelated high-frequency excess amplitude noise and because first experiments with a synchronously pumped ring cavity showed less noise. However, we only observed a small decrease

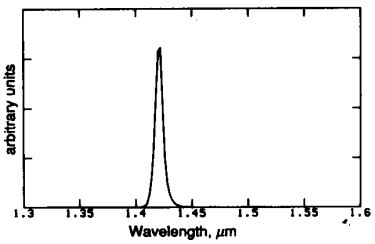

Fig. 11. Measured spectrum of the compressed pulses from a synchronously pumped configuration operating close to the single-pass compressor threshold.

of noise in the synchronously pumped ring cavity because of the high losses, which reduces the cavity lifetime. The noise is generated by many spontaneously Raman-shifted photons, which are relaunched into the fiber and act as seeders for the Raman gain. This is why the synchronously pumped laser gives only a small reduction of the amplitude noise in comparison to the single-pass compressor. For a further decrease in amplitude noise, much less cavity loss would be required, making a fully integrated synchronously pumped cavity necessary. A pump laser with a tunable repetition rate for the synchronization of the two laser cavities is recommended because an integrated adjustable delay line may be difficult to fabricate. The observed increased pedestal power may add some additional problems.

A single-pass fiber Raman soliton compressor is a very simple method of achieving sub-200 fs time resolution, making it attractive for optical pump–probe experiments with large signal levels. However, better noise properties are required for small signal measurements, such as electrooptic and charge-sensing sampling measurements, for which a fully integrated synchronously pumped fiber Raman soliton laser might be a solution.

Acknowledgment

The single-mode fiber was donated by Corning Glass Works through their university gift program. The polarization-preserving fiber was provided by K. Okamoto from NTT Japan. The fast InGaAs p-i-n photodiode was supplied by S. Y. Wang from Hewlett-Packard Laboratories. The authors thank M. N. Islam (AT&T Bell Laboratories), J. R. Taylor (Imperial College, London), and J. D. Kafka (Spectra Physics) for helpful discussions. U. Keller thanks D. H. Auston, M. C. Nuss, and J. A. Valdmanis for their guidance with subpicosecond laser systems during a summer program at AT&T Bell Laboratories, Murray Hill, NJ, in 1986.

References

[1] R. H. Stolen, "Fiber Raman lasers," in *Fiber and Integrated Optics, Vol. 3*. Crane, Russak, Co., 1980, pp. 21–25.

[2] L. F. Mollenauer, R. H. Stolen, and J. P. Gorden, "Extreme picosecond pulse narrowing by means of soliton effect in single-mode optical fibers," *Opt. Lett.*, vol. 8, pp. 289–291, 1983.

[3] A. S. Gouveia-Neto, A. S. L. Gomes, and J. R. Taylor, "Femtosecond soliton Raman generation," *IEEE J. Quantum Electron.*, vol. QE-24, pp. 332–340, 1988.

[4] J. D. Kafka and T. Baer, "Fiber Raman soliton laser pumped by a Nd:YAG laser," *Opt. Lett.*, vol. 12, pp. 181–183, 1987.

[5] M. N. Islam, L. F. Mollenauer, and R. H. Stolen, "Fiber Raman amplification soliton laser (FRASL)," in *Ultrafast Phenomena V, Springer Ser. Chem. Phys., Vol. 46*, G. R. Fleming and A. E. Siegman, Eds. Berlin: Springer-Verlag, 1986, pp. 46–50.

[6] B. Zysset, P. Beaud, and W. Hodel, "Generation of optical solitons in the wavelength region 1.37–149 μm," *Appl. Phys. Lett.*, vol. 50, pp. 1027–1029, 1987.

[7] K. J. Weingarten, M. J. W. Rodwell, and D. M. Bloom, "Picosecond optical sampling of GaAs integrated circuits," *IEEE J. Quantum Electron.*, vol. 24, pp. 198–220, 1988.

[8] H. K. Heinrich, D. M. Bloom, and B. R. Hemenway, "Noninvasive sheet charge density probe for integrated silicon devices," *Appl. Phys. Lett.*, vol. 48, pp. 1066–1068, 1986.

[9] U. Keeler, S. K. Diamond, B. A. Auld, and D. M. Bloom, "A noninvasive optical probe of free charge and applied voltage in GaAs devices," *Appl. Phys. Lett.*, vol. 53, pp. 388–390, 1988.

[10] U. Keller, J. A. Valdmanis, M. C. Nuss, and A. M. Johnson, "53 ps pulses at 1.32 μm from a harmonic mode-locked Nd:YAG laser," *IEEE J. Quantum Electron.*, vol. 24, pp. 427–430, 1988.

[11] "Spectrum analysis . . . Noise measurements," Hewlett-Packard Co., Palo Alto, CA, Appl. Note AN 246-2.

[12] "Measuring phase noise with the HP 3585A spectrum analyzer," Hewlett-Packard Co., Palo Alto, CA, Appl. Note AN 246-2.

[13] "Phase noise characterization of microwave oscillators," Frequency Discriminator Method, Hewlett-Packard Co., Palo Alto, CA, Product Note 11729C-2.

[14] D. von der Linde, "Characterization of the noise in continuosly operating mode-locked lasers," *Appl. Phys. B*, vol. 39, pp. 201–217, 1986.

[15] M. J. W. Rodwell, K. J. Weingarten, D. M. Bloom, T. Baer, and B. H. Kolner, "Reduction of timing fluctuations in a mode-locked Nd:YAG laser by electronic feedback," *Opt. Lett.*, vol. 11, pp. 638–640, 1986.

[16] J. Kluge, D. Wiechert, and D. von der Linde, "Fluctuations in synchronously mode-locked dye lasers," *Opt. Commun.*, vol. 51, pp. 271–277, 1984.

[17] D. F. Walls, "Squeezed states of light," *Nature*, vol. 306, pp. 141–146, 1983.

[18] R. H. Stolen and A. M. Johnson, "The effect of pulse walk off on stimulated Raman scattering in fibers," *IEEE J. Quantum Electron.*, vol. QE-22, pp. 2154–2160, 1986.

Ursula Keller was born June 21, 1959 in Zug, Switzerland. She received the Diplom in experimental physics from the Federal Institute of Technology (ETH) Zürich, Switzerland in 1984 and the M.S. degree in applied physics from Stanford University, Stanford, CA, in 1987.

From 1984 to 1985 she was a postgraduate researcher working on optical bistability at Heriot-Watt University, Edinburgh, Scotland, with Prof. S. D. Smith. Currently, she is a Ph.D. candidate in applied physics at Stanford University, working with Prof. D. M. Bloom. During 1985–1986 she was a Fulbright Fellow and in 1987–1988 she received an IBM Predoctoral Fellowship. Her research is in optical probing of electronic devices, especially charge sensing in GaAs devices, and low-noise, subpicosecond optical pulse generation in the near infrared.

Kathryn D. Li was born in Red Bank, NJ, on October 4, 1965. She received the A.B. degree in the physics/engineering program from Princeton University, Princeton, NJ, in 1987.

Since then, she has been working towards the Ph.D. degree in the applied physics at Stanford University, Stanford, CA. Her research with Prof. D. M. Bloom in the Edward L. Ginzton Laboratory concerns the use of lasers with fast devices. She is currently a Hertz Fellow and a recipient of an AT&T Graduate Research Program for Women Grant.

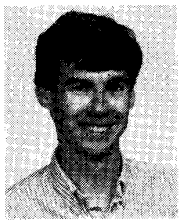

Mark Rodwell was born on January 18, 1960, in Altrincham, England. He received the B.S. degree in electrical engineering from the University of Tennessee, Knoxville, in 1980, and the M.S. and Ph.D. degrees in electrical engineering, from Stanford University, Stanford, CA, in 1982 and 1988, respectively.

From 1982 through 1984 he was with AT&T Bell Laboratories, designing fiber-optic digital transmission systems. In 1984 he returned to Stanford University to pursue research in electrooptic sampling of GaAs integrated circuits, picosecond electrical pulse generation, and picosecond electronic sampling. He remained at Stanford as a Research Associate until September 1988. Currently, he is an Assistant Professor with the Department of Electrical and Computer Engineering, University of California, Santa Barbara. His current research interests are picosecond electronic and optoelectronic devices and circuits, millimeter-wave integrated circuits, and picosecond instrumentation.

David M. Bloom (S'68-M'76-M'80-SM'86-F'87) was born on October 10, 1948, in Brooklyn, NY. He received the B.S. degree in electrical engineering from the University of California, Santa Barbara, in 1970 and the M.S. and the Ph.D. degrees in electrical engineering from Stanford University, Stanford, CA, in 1972 and 1975, respectively.

From 1975 to 1977 he was employed by Stanford University as a Research Associate. During this period he was awarded the IBM Postdoctoral Fellowship. From 1977 to 1979 he was employed by Bell Telephone Laboratories, Holmdel, NJ, where he conducted research on optical phase conjugation, ultrafast optical pulse propagation in fibers, and tunable color-center lasers. From 1979 to 1983 he served on the staff and later as a Project Manager at Hewlett-Packard Laboratories, Palo Alto, CA. While there he conducted and managed research on fiber optical devices, high-speed photodetectors, and picosecond electronic measurement techniques. In late 1983 he joined the Edward L. Ginzton Laboratory, W. W. Hansen Laboratories of Physics, Stanford University, where he is currently an Associate Professor of Electrical Engineering. His current research interests are ultrafast optics and electronics.

Prof. Bloom was awarded the 1980 Adolph Lomb Medal of the Optical Society of America for his pioneering work on the use of nonlinear optical processes to achieve real time conjugate wavefront generation. In 1981 he was elected a Fellow of the Optical Society of America in recognition of his distinguished service in the advancement of optics. He was the 1985 IEEE LEOS Traveling Lecturer. In 1986 he was elected a Fellow of the IEEE for contributions to nonlinear optics and ultrafast optoelectronics.